Report

Cell Reports

Manipulating Hippocampal Place Cell Activity by Single-Cell Stimulation in Freely Moving Mice

Graphical Abstract

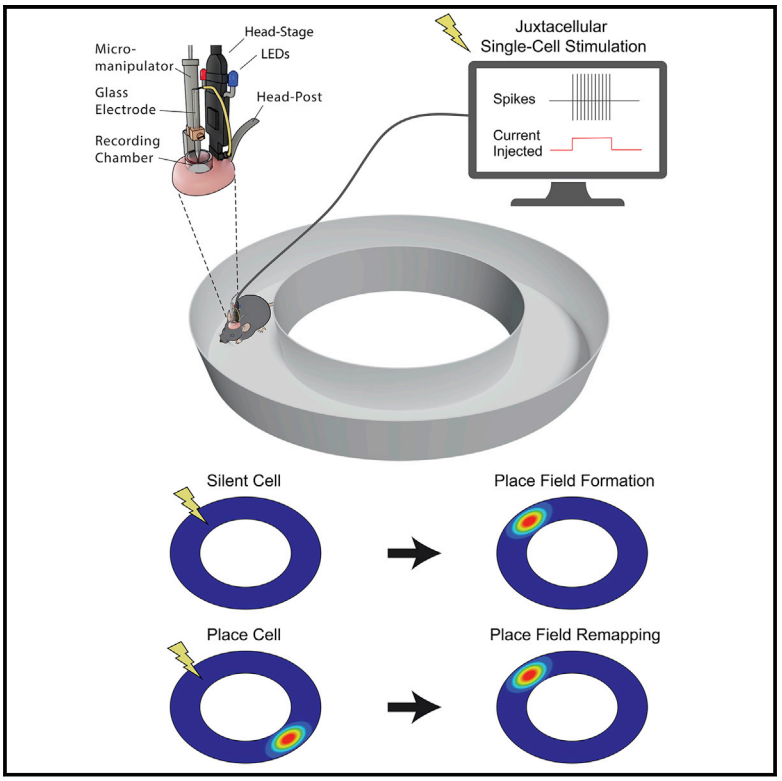

Authors

Maria Diamantaki, Stefano Coletta, Khaled Nasr, ..., Philipp Berens, Patricia Preston-Ferrer, Andrea Burgalossi

Correspondence

andrea.burgalossi@cin.uni-tuebingen.de

In Brief

Place cells can serve as a readout of hippocampal memory. Diamantaki et al. show that the activity of single place cells can be rapidly modified by single-cell stimulation in freely moving mice. This finding provides insights into the cellular mechanisms that support the rapid reorganization of hippocampal place maps.

Highlights

- Juxtacellular stimulation of single hippocampal neurons in freely moving mice
- Stimulation in silent neurons can induce place fields
- Stimulation in single place cells can induce place field remapping

Diamantaki et al., 2018, Cell Reports *23*, 32–38
April 3, 2018
https://doi.org/10.1016/j.celrep.2018.03.031

CellPress

OPEN ACCESS
CellPress

Cell Reports
Report

Manipulating Hippocampal Place Cell Activity by Single-Cell Stimulation in Freely Moving Mice

Maria Diamantaki,[1,2,4] Stefano Coletta,[1,2,4] Khaled Nasr,[1,2] Roxana Zeraati,[1,2] Sophie Laturnus,[1,3] Philipp Berens,[1,3] Patricia Preston-Ferrer,[1] and Andrea Burgalossi[1,5,*]

[1]Werner-Reichardt Centre for Integrative Neuroscience, Otfried-Müller-str. 25, 72076 Tübingen, Germany
[2]Graduate Training Centre of Neuroscience—IMPRS, 72074 Tübingen, Germany
[3]Institute of Ophthalmic Research, University of Tübingen, Tübingen, Germany
[4]These authors contributed equally
[5]Lead Contact
*Correspondence: andrea.burgalossi@cin.uni-tuebingen.de
https://doi.org/10.1016/j.celrep.2018.03.031

SUMMARY

Learning critically depends on the ability to rapidly form and store non-overlapping representations of the external world. In line with their postulated role in episodic memory, hippocampal place cells can undergo a rapid reorganization of their firing fields upon contextual manipulations. To explore the mechanisms underlying such global remapping, we juxtacellularly stimulated 42 hippocampal neurons in freely moving mice during spatial exploration. We found that evoking spike trains in silent neurons was sufficient for creating place fields, while in place cells, juxtacellular stimulation induced a rapid remapping of their place fields to the stimulus location. The occurrence of complex spikes was most predictive of place field plasticity. Our data thus indicate that plasticity-inducing stimuli are able to rapidly bias place cell activity, simultaneously suppressing existing place fields. We propose that such competitive place field dynamics could support the orthogonalization of the hippocampal map during global remapping.

INTRODUCTION

Neural circuits are thought to encode information via rapid and long-lasting modifications of synaptic weights. According to the Hebbian learning theory (Hebb, 1961), inputs that persistently take part in firing of a postsynaptic neuron become potentiated. This type of plasticity is referred to as input specific (or homosynaptic), because it critically depends on the near-simultaneous co-activation of pre- and postsynaptic neurons with specific temporal ordering rules (Markram et al., 1997; Abbott and Nelson, 2000; Bittner et al., 2017). Experimentally, these mechanisms have been extensively studied in the hippocampus, a brain region that has been strongly implicated in learning and memory. After the discovery of associative learning rules (Bliss and Lømo, 1973), it was found that the input activation should be strong and exceed a certain threshold to induce plastic changes (cooperativity rule) (McNaughton et al., 1978). Episodes of strong postsynaptic activity can also lead to concomitant weakening (or de-potentiation) of synapses that were not active during the induction, a process known as heterosynaptic plasticity (Lynch et al., 1977; Chistiakova et al., 2014). It has been shown that both forms of plasticity (homo- and heterosynaptic) can occur simultaneously on the same neuron (Volgushev et al., 1997; Lee et al., 2012; Chen et al., 2013), thus playing an important role in supporting synaptic competition (Miller, 1996; Elliott and Shadbolt, 2002; Finelli et al., 2008) and in preventing the saturation of synaptic weights (Kempter et al., 2001; Wu and Yamaguchi, 2006). Thus, the bidirectional regulation of synaptic weights via homo- and heterosynaptic plasticity mechanisms, operating on the same scale, is necessary for supporting learning within hippocampal circuits.

The seminal discovery of place cells (O'Keefe and Dostrovsky, 1971)—neurons that become active in a specific location of the environment visited by the animal—has provided fundamental insights into hippocampal function during natural behavior. During spatial exploration, the collective activity of place cells forms a map-like representation of the external space. These maps form rapidly during exploration of a novel environment (Hill, 1978; Wilson and McNaughton, 1993; Frank et al., 2004; Cohen et al., 2017) and remain stable over many consequent exposures to the same environment (Muller and Kubie, 1987; Frank et al., 2004; Dupret et al., 2010). However, when exposed to a different context, place cells have the capability of undergoing rapid reorganization of their firing fields so that a new spatial map is instantiated collectively (Muller and Kubie, 1987; Muller et al., 1991). By this process (known as global remapping), a large number of orthogonal maps can be created within the hippocampus (Alme et al., 2014; Rich et al., 2014) thus satisfying the high-capacity requirements of a memory network (Battaglia and Treves, 1998; Colgin et al., 2008).

The capability of rapidly forming orthogonal representations is therefore crucial for memory and hippocampal function. Studies have shown that place field activity can emerge from silent neurons by manipulations of activity and/or excitability (Lee et al., 2012; Bittner et al., 2015, 2017; Diamantaki et al., 2016a) and that manipulations of upstream entorhinal inputs (Miao et al., 2015; Rueckemann et al., 2016; Kanter et al., 2017) or local place cell activity (Schoenenberger et al., 2016; Trouche et al., 2016) can induce hippocampal remapping. However, the cellular mechanisms underlying the rapid

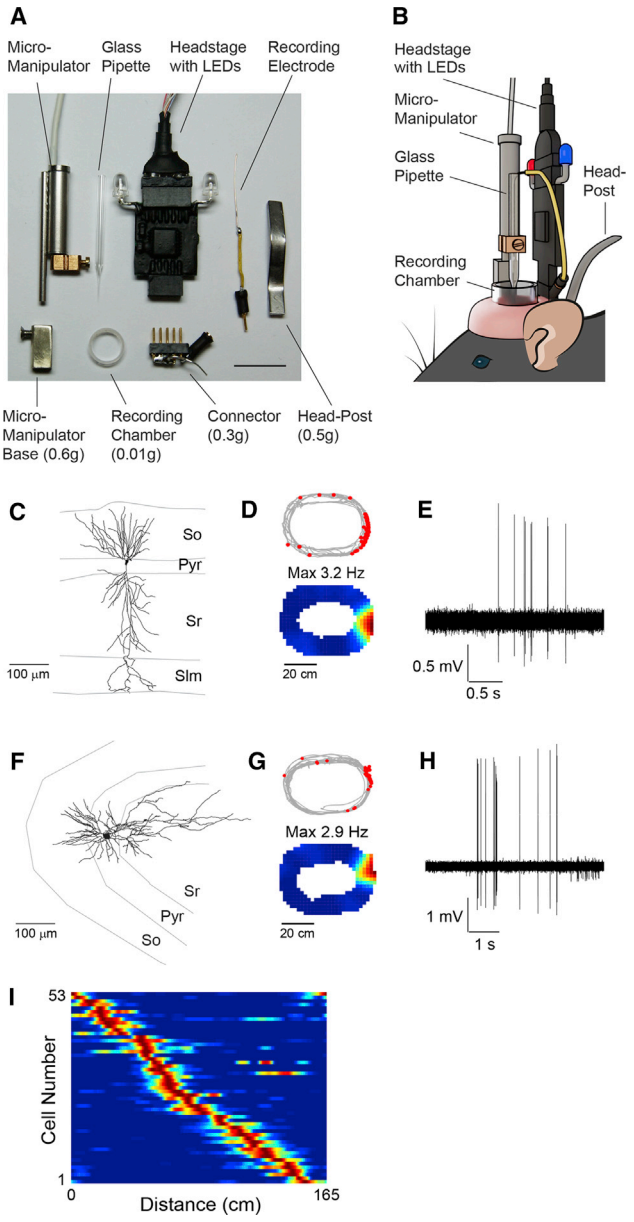

Figure 1. Juxtacellular Recordings and Identification of Single Hippocampal Neurons in Freely Moving Mice

(A) Individual implant components that are either cemented to (head post, connector, recording chamber, and micromanipulator base) or mounted on (head stage, micromanipulator, glass pipette, and silver-wire recording electrode) the mouse's head before recording. The respective weights of the custom-made components are indicated. Scale bar, 1 cm.

(B) Schematic drawing of the fully assembled recording implant on the animal's head.

(C) Reconstruction of the dendritic morphology of a CA1 pyramidal neuron, recorded in a freely moving mouse (recording shown in D). Sr, stratum radiatum; Pyr, stratum pyramidale; So, stratum oriens; Slm, stratum lacunosum moleculare.

(D) Spike-trajectory plots (top) and rate maps (bottom) for the neuron shown in (C). Spontaneous spikes (red dots) and maximal firing rates are indicated.

(E) Representative high-pass filtered spike trace for the recordings shown in (D).

(F–H) Same as in (C)–(E) except for an identified CA3 pyramidal neuron.

(I) Color-coded distribution of place fields for all place cells (n = 53). Each row represents the normalized firing rates relative to the linearized 1D projection of the circular arena. Cells are ordered according to their place field position along the linearized trajectory.

reorganization of spatial activity in hippocampal place cells have remained largely unexplored.

Here we sought to address this question by employing juxtacellular stimulation of individual hippocampal neurons in the intact system, i.e., in freely moving mice engaged in spatial exploration. We provide evidence that juxtacellular stimulation in single place cells can lead to the rapid remapping of their place fields to the stimulus location. This input-based mechanism might support the rapid reorganization of the place map during global remapping.

RESULTS

Juxtacellular Recording Procedures in Freely Moving Mice

To record and stimulate single hippocampal neurons in freely moving mice, we adapted our juxtacellular procedures—developed and optimized in rats (Tang et al., 2014)—to mice. Animals were implanted with miniaturized components, including a head post, micromanipulator base, recording chamber, and connector (Figures 1A and 1B; Figures S1A and S1B), whose size and total weight (~1.4 g) were reduced to fit within the typical range of extracellular implants for mice (Jiang et al., 2017). Compared to the components previously used for rats (Tang et al., 2014; Diamantaki et al., 2016a, 2016b), the fully assembled recording implant contained a more compact micromanipulator-base assembly and a smaller head stage (Figures 1A and 1B; Figures S1A and S1B). During unrestrained behavior, the weight of the recording assembly was offset by a counterbalance system (see Supplemental Information for details).

We then employed juxtacellular recording procedures to monitor the activity of single neurons in the dorsal hippocampus (CA1 and CA3 subfields) while mice explored a familiar circular arena. Figures 1C–1H show two representative recordings from an identified CA1 pyramidal neuron (Figures 1C–1E) and an identified CA3 pyramidal cell (Figures 1F–1H), both of which displayed spatially localized spiking patterns (Figures 1D and 1G), a defining signature of place cell activity. Altogether, we recorded the activity of 87 hippocampal neurons during spatial exploration. In line with previous extracellular studies (Wilson and McNaughton, 1993; Lee et al., 2004; Leutgeb et al., 2004; Preston-Ferrer and Burgalossi, 2017), most of these active cells displayed spatially localized activity (~60%; 53 of 87 active neurons classified as place cells) (see details in Supplemental Information), and the firing fields of the place cell population evenly covered the available space (Figure 1I). All neurons included in the present study displayed low firing rates (<10 Hz; average firing rate = 2.33 ± 2.40 Hz; n = 87) and often fired short bursts of action potentials (referred to as complex spikes) (average burst index = 0.13 ± 0.12; n = 87)—features classically associated with principal cell identity (O'Keefe and Dostrovsky, 1971; Ranck, 1973). Cell identification by juxtacellular labeling confirmed these standard electrophysiological

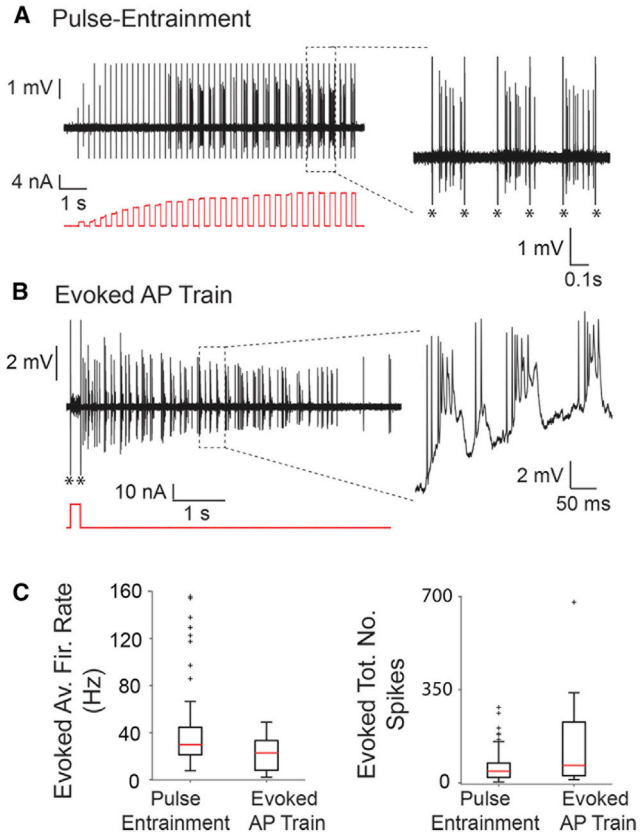

Figure 2. Single-Cell Stimulation Procedures in Freely Moving Mice

(A) Representative high-pass filtered voltage trace (top) showing the activity of a single neuron in response to a pulse-entrainment stimulation protocol (current trace in red, bottom). The intensity of the 200 ms square current pulses was adjusted online to reach the threshold necessary to evoke action potentials (from the ninth pulse onward in this representative example). Right, high magnification showing entrainment of spiking activity by the current pulses. Asterisks indicate stimulus artifacts, truncated for display.

(B) Representative high-pass filtered voltage trace (top) showing an evoked spike train, which outlasted the square current pulse (current trace in red, bottom). Right, high magnification showing the presence of complex spikes. Asterisks indicate stimulus artifacts, truncated for display.

(C) Boxplots showing evoked average firing rates and total number of spikes for pulse entrainment (n = 60) and evoked action potential trains (n = 23). Whiskers represent a 1.5 interquartile range. Outliers are shown as crosses.

classification criteria in that all identified neurons for which morphology could be assessed (15 of 22 identified neurons) were classified as pyramidal cells (see details in Supplemental Information).

Juxtacellular recordings in mice displayed a higher degree of mechanical stability compared to recordings performed in rats (Tang et al., 2014). In multiple occasions, it was possible to maintain a juxtacellular recording from a single neuron while releasing the animal from head fixation and transferring it to the behavioral arena. Figures S1C and S1E show a representative example in which a recording from a hippocampal neuron, established under head fixation, could be maintained while the animal was released, lifted, and gently placed into the behavioral arena. During exploration, the neuron displayed place cell activity (Figure S1C). The higher mechanical stability of juxtacellular recordings in mice also made it possible to transfer animals from one arena to another while sequentially monitoring the activity of the same neuron. This is shown in the representative recording in Figures S1D and S1F, in which a hippocampal neuron, which was largely silent in a familiar circular arena (only 3 spikes in 80.4 s; average firing rate = 0.037 Hz), displayed spatially localized activity in a novel square environment (Figure S1D). At the end of the recording, the neuron was labeled and identified as a deep CA1 pyramidal neuron (data not shown).

Altogether, these data indicate that juxtacellular recording procedures can be employed for monitoring the activity of hippocampal neurons in freely moving mice with a high degree of mechanical stability.

Juxtacellular Stimulation of Single Hippocampal Neurons during Spatial Exploration

Next, we tested whether hippocampal representations in mice engaged in unrestrained natural behavior (i.e., spatial exploration) can be modified by single-cell manipulations of spiking activity. To this end, we employed standard juxtacellular stimulation procedures, referred to as nanostimulation by previous authors (Houweling and Brecht, 2008; Houweling et al., 2010; Doron et al., 2014; Stüttgen et al., 2017), in which squared current pulses are delivered to the recorded neuron to elicit spikes (Figure 2) (see Supplemental Information for details). In line with previous work (Houweling et al., 2010), when applied to cortical neurons under anesthesia, this stimulation protocol enabled parametric control of evoked action potential number and frequency (as in Houweling et al., 2010; Doron et al., 2014) (data not shown). However, the same protocol led to less consistent entrainment of spiking activity in hippocampal cells during unrestrained behavior, possibly due to intrinsic cell-type differences and/or more variable loose-seal configurations compared to more mechanically stable preparations. In most cases (39 of 62 stimulations), it was possible to entrain the activity of single hippocampal neurons in freely moving mice so that evoked spikes were largely confined to the stimulation pulses (Figure 2A); however, in some cases (23 of 62 stimulations), longer spike trains were triggered that outlasted the stimulation pulse (Figure 2B). These evoked spike trains often contained bursts of action potentials, which appeared as complex spikes associated to underlying dendritic plateau potentials (Epsztein et al., 2011; Bittner et al., 2015). We will refer to these events as evoked complex spikes.

We then employed these stimulation procedures for evoking spikes in hippocampal neurons while animals were freely exploring a familiar circular arena. Stimulation-evoked spiking activity parameters (e.g., average firing rates and total number of spikes) (Figure 2C) varied across stimulations during both pulse entrainment (evoked firing rates, median = 29.5 Hz, interquartile range = 23.2 Hz; total number of spikes, median = 44, interquartile range = 54) and evoked action potential (AP) trains (average firing rates, median = 22.5 Hz, interquartile range = 25.1 Hz; total number of spikes, median = 66, interquartile range = 202). In line with observations from freely moving rats (Diamantaki et al., 2016a), we found that juxtacellular stimulation was able to prime the rapid appearance of

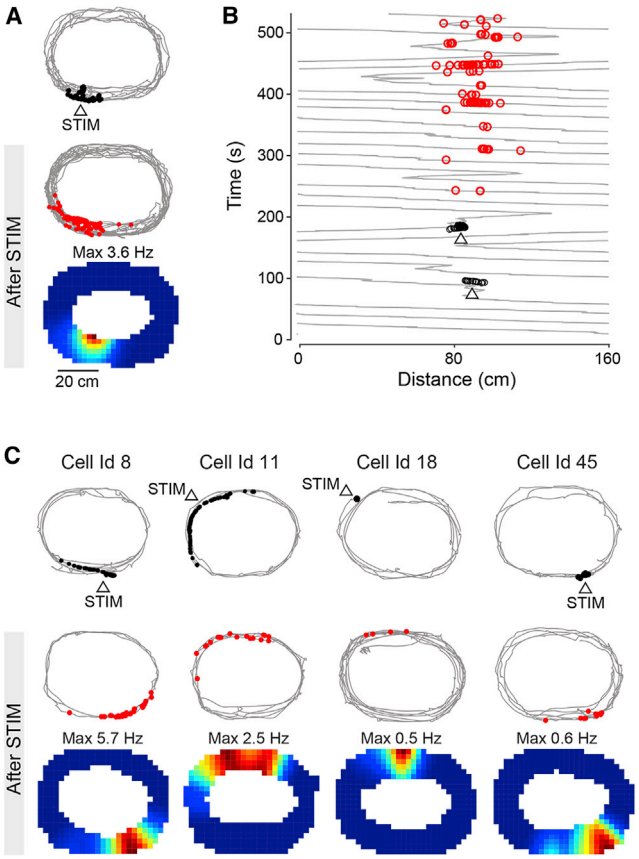

Figure 3. Juxtacellular Stimulation Can Evoke Spatial Activity in Silent Hippocampal Neurons

(A) Top, spike-trajectory plot before and during stimulation (arrowhead). Bottom, spike-trajectory plot and rate map after stimulation. Stimulus spikes (black dots), spontaneous spikes after the stimulation (red dots), and maximal firing rate are indicated.

(B) Lap-by-lap analysis for the recording shown in (A). Stimulus spikes (black circles, indicated by the arrowhead) and spontaneous spikes (red circles) are indicated. The induced place field was stable for the entire recording (~12 laps after the stimulus train).

(C) Same as in (A) except for four additional representative neurons (cell ids indicated).

place fields in previously silent cells. This is shown in the representative recording in Figures 3A and 3B, in which juxtacellular stimulation of a silent neuron was sufficient for eliciting spatially localized activity at the stimulus location. Altogether, 22 silent neurons were stimulated at randomly chosen locations in freely moving mice, and in ~32% of them (7 of 22), spatial activity could be induced by juxtacellular stimulation (see additional examples in Figure 3C). Following stimulation, spontaneous activity at the stimulus location appeared rapidly (average latency = 55.6 ± 53.0 s) and often persisted until the end of the recordings (Figure 3B). This indicates that in line with previous evidence (Lee et al., 2012; Bittner et al., 2015; Diamantaki et al., 2016a), single-cell stimulation in silent hippocampal neurons can be sufficient for inducing the rapid appearance of place activity during unrestrained natural behavior.

Next, we tested the effect of out-of-field stimulations in single place cells. To this end, we evoked spikes outside place fields by juxtacellular stimulation (n = 20 stimulated neurons) (Figure 4) at an average distance of 46.5 ± 8.9 cm from the original place field. We found that in a consistent fraction of the stimulated cells (~45%; 9 of 20) place activity could be rapidly modified by juxtacellular stimulation. In most cases (n = 7), juxtacellular stimulation induced a remapping of the place field to the stimulus location (Figures 4A and 4B). That is, the original field disappeared (or became considerable weaker), while a new activity cluster emerged at the stimulus location (see also cell identifier [id] 25 and cell id38 in Figure 4C). In two other cases, we observed the appearance of an additional field (see cell id14 in Figure 4C). To quantify stimulation effects, we computed pixel-by-pixel correlations between rate maps before and those after stimulation. Rate-map correlations were bimodally distributed (Figure 4D), with the remapping group displaying low correlations (<0.05; n = 7) and the no-effect cells displaying high correlations (>0.62; n = 13), the exception being the two neurons in which an additional field was induced, which retained relatively high correlations (0.64 and 0.62) due to the persistence of the original place field (arrow in Figure 4D). At the population level, including all stimulated place cells (n = 20), single-cell stimulation resulted in a significant decrease of activity within the original place field (before, 8.3 ± 8.7 Hz; after, 5.9 ± 8.07 Hz; p = 0.02; Wilcoxon signed-rank test), while an increase was observed at the stimulus location (before, 0.09 ± 0.15 Hz; after, 0.99 ± 1.65 Hz; p = 0.009; Wilcoxon signed-rank test) (Figure 4E). Average firing rates before and after stimulation were not significantly different (before, 1.7 ± 1.3 Hz; after, 2.0 ± 2.0 Hz; p = 0.55; Wilcoxon signed-rank test), indicating that single-cell stimulation induced a redistribution of spatial firing rather than a global change in activity levels.

As for the induction of place fields in silent neurons (Figure 3), modifications of place activity were also fast (average latency, 99.3 ± 142.9 s) and often persisted until the end of the recording (Figure 4B). In one case, in which we could test the same neuron in the circular arena, in a square maze, and then back to the circular arena (Figure S2), we observed that the induced place field was still expressed on the second exposure to the circular arena (Figure S2D). However, in general, the limited recording durations (344 ± 485 s) and total number of laps (13.8 ± 11.2) prevented rigorous assessment of long-term effects of juxtacellular stimulation.

Lastly, we asked whether evoked spike-train parameters could be used to predict stimulation effects. In line with previous work (Bittner et al., 2015), we found that in 11 of 16 cells in which juxtacellular stimulation induced a place field (Figure 3) or place field remapping (Figure 4), complex spikes were observed. This proportion was significantly higher than in neurons without stimulation effects (3 of 26; p = 0.0004; Fisher's exact test). To confirm this observation, we used regularized logistic regression with recursive feature elimination (see Supplemental Information) and found that the presence of complex spikes within evoked spike trains was most predictive of a stimulation effect (Figure S3). This observation strengthens the view that evoked complex spikes are key plasticity-inducing events that can

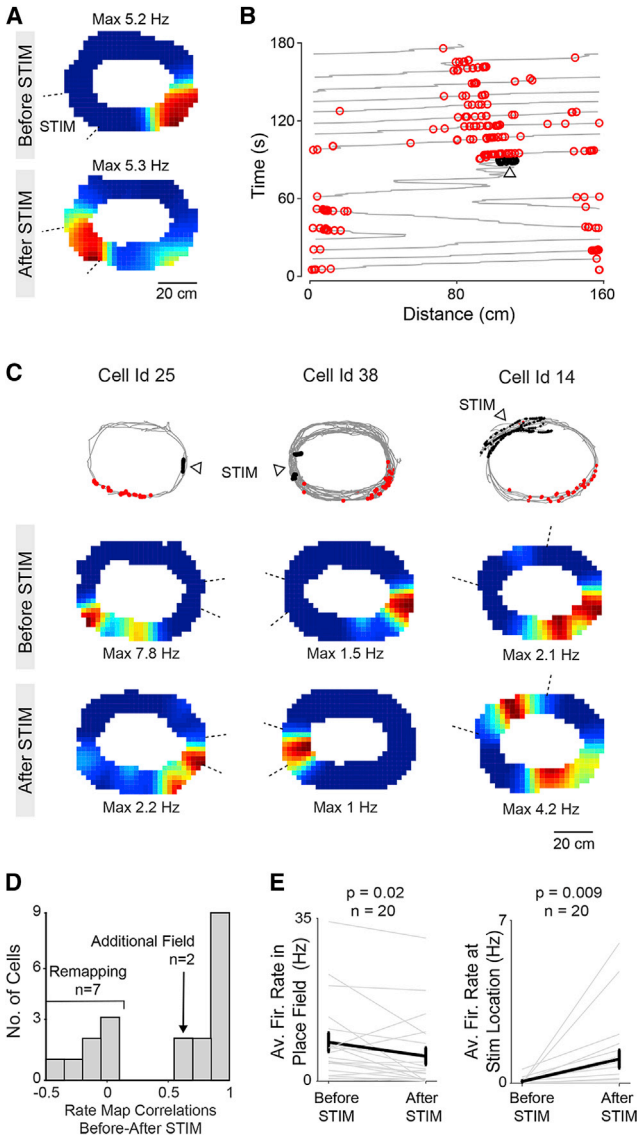

Figure 4. Out-of-Field Juxtacellular Stimulation of Hippocampal Place Cells Can Modify Spatial Tuning

(A) Spike-trajectory plot and rate maps computed before (top) and after (bottom) juxtacellular stimulation. The area containing the stimulus spikes is marked by dotted lines on the rate map. Maximal firing rates are indicated.

(B) Lap-by-lap analysis for the recording shown in (A). Stimulus spikes (black circles, indicated by the arrowhead) and spontaneous spikes (red circles) are indicated. The induced place field was stable for the entire recording (~9 laps after the stimulus train).

(C) Same as in (A) except for three additional representative neurons (cell ids indicated). Note the appearance of an additional place field in cell id14 and place field remapping toward the stimulus locations in cell id25 and cell id38.

(D) Histogram of the pixel-by-pixel correlation between rate maps computed before and those computed after stimulation (n = 20). Note the low map correlations in the subset of place cells in which the stimulation induced place field remapping (n = 7); the bin corresponding to the two neurons in which an additional place field was observed is indicated by the arrow.

(E) Average firing rate within the place field area (left) and the stimulus area (right) before and after stimulation (n = 20). Although a significant decrease was observed within the original place field, the opposite was the case within the stimulated area. The p values are indicated (Wilcoxon signed-rank test).

bias spatial activity—both in silent and in place cells—during spatial exploration.

DISCUSSION

In the present work, we show that juxtacellular stimulation of single hippocampal neurons can be sufficient for biasing neuronal output to the stimulus location. In line with previous evidence from head-fixed animals (Bittner et al., 2015) and freely moving animals (Diamantaki et al., 2016a), we show that spatially localized suprathreshold activation can recruit silent hippocampal neurons into the coding population. Overall, the probability of inducing place fields by juxtacellular stimulation in silent pyramidal neurons was relatively low (~32%). Although stimulation efficiencies could be higher in a novel environment (Diamantaki et al., 2016a), this was most likely due to the large variability in the evoked activity parameters (Figure 2C). Based on correlative evidence (Figure S3) and previous work (Bittner et al., 2015, 2017), we envision the possibility of precisely controlling the occurrence of complex spikes by juxtacellular stimulation resulting in higher efficiency in creating place fields (Figure 3) or inducing place field remapping (Figure 4) during unrestrained behavior.

Place fields can be virtually induced at any location visited by the animal (Figures 3 and 4), which indirectly suggests that place cells might receive a range of spatially tuned inputs, spanning the entire available space. This hypothesis is in line with intracellular studies (Lee et al., 2012; Bittner et al., 2015) and imaging studies (C. Domnisoru and D.W. Tank, 2017, Soc. Neurosci., abstract) that point to a broad distribution of input tuning in individual place cells. Such a random functional connectivity scheme would confer a high degree of flexibility in neural coding, enabling place cells to rapidly tune their output to changing subsets of potentiated inputs.

The most important finding of this study is perhaps the observation that individual place cells can undergo fast remapping in response to single-cell stimulation (Figure 4). Even under conditions in which the hippocampal map is thought to be most stable (i.e., in a familiar environment), the firing location of individual place cells can be dynamically biased by suprathreshold activation. Previous work has shown that hippocampal remapping can be triggered by manipulations of upstream inputs (Miao et al., 2015; Rueckemann et al., 2016; Kanter et al., 2017) and can occur in response to optogenetic-mediated inhibition of place cell activity (Schoenenberger et al., 2016; Trouche et al., 2016). Our data add to this work by showing that strong spatially localized stimuli are able to rapidly switch place field location in individual place cells. Mechanistically, this is consistent with a stimulation-induced potentiation of the spatial inputs active around the stimulus location (via homosynaptic plasticity) (Bittner et al., 2015, 2017) and a concomitant depotentiation of place-related activity (via heterosynaptic plasticity). This fast form of place field plasticity appears to be ideally suited for the instantiation of novel spatial maps during global remapping by ensuring that the emergence of novel place fields is accompanied by a concomitant weakening of the previous activity patterns. Such a mechanism would be particularly suited under conditions in which existing representations have to be flexibly

adapted to changing behavioral or contextual contingencies (e.g., Fyhn et al., 2002; Anderson and Jeffery, 2003; Dupret et al., 2010; Spiers et al., 2015). We envision that a new set of upstream inputs, if sufficiently strong to drive dendritic plateau potentials, could be sufficient for resetting place cell output and ensuring the rapid emergence of a new representation. Thus, the output of hippocampal neurons might be determined by the competitive interaction between inputs' strengths via a winner-takes-all mechanism.

In summary, we show that much like place cell remapping under natural conditions, juxtacellular stimulation can promote a rapid switch of place field location in single neurons. This cell-autonomous mechanism constrains current models of hippocampal remapping in that a transient redistribution of input strengths, rather than a global reorganization of inputs, might be sufficient for biasing the spatial output of hippocampal neurons. Methodologically, we show that juxtacellular techniques can also be employed in freely moving mice (Figure 1), offering the possibility of combining single-cell identification and stimulation with mouse genetics. This single-cell approach complements current virtual reality-based methods, by making it possible to probe the plasticity rules of spatial representations during natural multisensory-guided spatial behaviors.

EXPERIMENTAL PROCEDURES

Animals

All experimental procedures were performed according to the German guidelines on animal welfare under the supervision of local ethics committees. Surgery and implantation on wild-type C57BL/6J mice (males, >2 months old; Charles River) were performed following previously published procedures (Tang et al., 2014).

Juxtacellular Recordings

Juxtacellular recordings, signal acquisition and processing, and animal tracking were essentially performed as previously described (Tang et al., 2014; Diamantaki et al., 2016a), as were juxtacellular stimulation of single neurons (referred to as nanostimulation) (Houweling and Brecht, 2008; Houweling et al., 2010; Doron et al., 2014) and single-cell labeling (Pinault, 1996; Preston-Ferrer et al., 2016).

Statistical Analysis

Statistical significance was assessed by Wilcoxon signed-rank test with 95% confidence intervals. Logistic regression classification with L2 regularization was performed by using the *glmnet* toolbox for Python. All data are presented as mean ± SD unless indicated otherwise.

Detailed methods can be found in Supplemental Information.

SUPPLEMENTAL INFORMATION

Supplemental Information includes STAR Methods and three figures and can be found with this article online at https://doi.org/10.1016/j.celrep.2018.03.031.

ACKNOWLEDGMENTS

This work was supported by the Werner Reichardt Centre for Integrative Neuroscience (CIN) at the Eberhard Karls University of Tübingen (CIN is an excellence cluster funded by the Deutsche Forschungsgemeinschaft [DFG] within the framework of the Excellence Initiative EXC 307), DFG grants BU 3126/1-1 and BE 5601/4-1, the SFB 1233 "Robust Vision," and the Bernstein Award for Computational Neuroscience (BMBF) (01GQ1601). We thank Alexandra Eritja for excellent assistance with anatomy experiments and Shimpei Ishiyama for illustrations.

AUTHOR CONTRIBUTIONS

A.B. and P.P.-F. conceived, designed, and supervised the study. A.B., M.D., and S.C. performed experiments. M.D., K.N., R.Z., and S.C. analyzed data. P.P.-F. analyzed anatomical data. S.L. and P.B. performed the classification analysis. A.B. wrote the manuscript, with input from all authors.

DECLARATION OF INTERESTS

The authors declare no competing interests.

Received: December 8, 2017
Revised: March 1, 2018
Accepted: March 8, 2018
Published: April 3, 2018

REFERENCES

Abbott, L.F., and Nelson, S.B. (2000). Synaptic plasticity: taming the beast. Nat. Neurosci. *3* (*Suppl*), 1178–1183.

Alme, C.B., Miao, C., Jezek, K., Treves, A., Moser, E.I., and Moser, M.-B. (2014). Place cells in the hippocampus: eleven maps for eleven rooms. Proc. Natl. Acad. Sci. USA *111*, 18428–18435.

Anderson, M.I., and Jeffery, K.J. (2003). Heterogeneous modulation of place cell firing by changes in context. J. Neurosci. *23*, 8827–8835.

Battaglia, F.P., and Treves, A. (1998). Stable and rapid recurrent processing in realistic autoassociative memories. Neural Comput. *10*, 431–450.

Bittner, K.C., Grienberger, C., Vaidya, S.P., Milstein, A.D., Macklin, J.J., Suh, J., Tonegawa, S., and Magee, J.C. (2015). Conjunctive input processing drives feature selectivity in hippocampal CA1 neurons. Nat. Neurosci. *18*, 1133–1142.

Bittner, K.C., Milstein, A.D., Grienberger, C., Romani, S., and Magee, J.C. (2017). Behavioral time scale synaptic plasticity underlies CA1 place fields. Science *357*, 1033–1036.

Bliss, T.V., and Lømo, T. (1973). Long-lasting potentiation of synaptic transmission in the dentate area of the anaesthetized rabbit following stimulation of the perforant path. J. Physiol. *232*, 331–356.

Chen, J.-Y., Lonjers, P., Lee, C., Chistiakova, M., Volgushev, M., and Bazhenov, M. (2013). Heterosynaptic plasticity prevents runaway synaptic dynamics. J. Neurosci. *33*, 15915–15929.

Chistiakova, M., Bannon, N.M., Bazhenov, M., and Volgushev, M. (2014). Heterosynaptic plasticity: multiple mechanisms and multiple roles. Neuroscientist *20*, 483–498.

Cohen, J.D., Bolstad, M., and Lee, A.K. (2017). Experience-dependent shaping of hippocampal CA1 intracellular activity in novel and familiar environments. eLife *6*, e23040.

Colgin, L.L., Moser, E.I., and Moser, M.-B. (2008). Understanding memory through hippocampal remapping. Trends Neurosci. *31*, 469–477.

Diamantaki, M., Frey, M., Preston-Ferrer, P., and Burgalossi, A. (2016a). Priming spatial activity by single-cell stimulation in the dentate gyrus of freely moving rats. Curr. Biol. *26*, 536–541.

Diamantaki, M., Frey, M., Berens, P., Preston-Ferrer, P., and Burgalossi, A. (2016b). Sparse activity of identified dentate granule cells during spatial exploration. eLife *5*, e20252.

Doron, G., von Heimendahl, M., Schlattmann, P., Houweling, A.R., and Brecht, M. (2014). Spiking irregularity and frequency modulate the behavioral report of single-neuron stimulation. Neuron *81*, 653–663.

Dupret, D., O'Neill, J., Pleydell-Bouverie, B., and Csicsvari, J. (2010). The reorganization and reactivation of hippocampal maps predict spatial memory performance. Nat. Neurosci. *13*, 995–1002.

Elliott, T., and Shadbolt, N.R. (2002). Multiplicative synaptic normalization and a nonlinear Hebb rule underlie a neurotrophic model of competitive synaptic plasticity. Neural Comput. *14*, 1311–1322.

Epsztein, J., Brecht, M., and Lee, A.K. (2011). Intracellular determinants of hippocampal CA1 place and silent cell activity in a novel environment. Neuron *70*, 109–120.

Finelli, L.A., Haney, S., Bazhenov, M., Stopfer, M., and Sejnowski, T.J. (2008). Synaptic learning rules and sparse coding in a model sensory system. PLoS Comput. Biol. *4*, e1000062.

Frank, L.M., Stanley, G.B., and Brown, E.N. (2004). Hippocampal plasticity across multiple days of exposure to novel environments. J. Neurosci. *24*, 7681–7689.

Fyhn, M., Molden, S., Hollup, S., Moser, M.-B., and Moser, E. (2002). Hippocampal neurons responding to first-time dislocation of a target object. Neuron *35*, 555–566.

Hebb, D. (1961). Organization of Behavior (Science Editions).

Hill, A.J. (1978). First occurrence of hippocampal spatial firing in a new environment. Exp. Neurol. *62*, 282–297.

Houweling, A.R., and Brecht, M. (2008). Behavioural report of single neuron stimulation in somatosensory cortex. Nature *451*, 65–68.

Houweling, A.R., Doron, G., Voigt, B.C., Herfst, L.J., and Brecht, M. (2010). Nanostimulation: manipulation of single neuron activity by juxtacellular current injection. J. Neurophysiol. *103*, 1696–1704.

Jiang, Z., Huxter, J.R., Bowyer, S.A., Blockeel, A.J., Butler, J., Imtiaz, S.A., Wafford, K.A., Phillips, K.G., Tricklebank, M.D., Marston, H.M., and Rodriguez-Villegas, E. (2017). TaiNi: Maximizing research output whilst improving animals' welfare in neurophysiology experiments. Sci. Rep. *7*, 8086.

Kanter, B.R., Lykken, C.M., Avesar, D., Weible, A., Dickinson, J., Dunn, B., Borgesius, N.Z., Roudi, Y., and Kentros, C.G. (2017). A novel mechanism for the grid-to-place cell transformation revealed by transgenic depolarization of medial entorhinal cortex layer II. Neuron *93*, 1480–1492.e6.

Kempter, R., Gerstner, W., and van Hemmen, J.L. (2001). Intrinsic stabilization of output rates by spike-based Hebbian learning. Neural Comput. *13*, 2709–2741.

Lee, I., Yoganarasimha, D., Rao, G., and Knierim, J.J. (2004). Comparison of population coherence of place cells in hippocampal subfields CA1 and CA3. Nature *430*, 456–459.

Lee, D., Lin, B.-J., and Lee, A.K. (2012). Hippocampal place fields emerge upon single-cell manipulation of excitability during behavior. Science *337*, 849–853.

Leutgeb, S., Leutgeb, J.K., Treves, A., Moser, M.-B., and Moser, E.I. (2004). Distinct ensemble codes in hippocampal areas CA3 and CA1. Science *305*, 1295–1298.

Lynch, G.S., Dunwiddie, T., and Gribkoff, V. (1977). Heterosynaptic depression: a postsynaptic correlate of long-term potentiation. Nature *266*, 737–739.

Markram, H., Lübke, J., Frotscher, M., and Sakmann, B. (1997). Regulation of synaptic efficacy by coincidence of postsynaptic APs and EPSPs. Science *275*, 213–215.

McNaughton, B.L., Douglas, R.M., and Goddard, G.V. (1978). Synaptic enhancement in fascia dentata: cooperativity among coactive afferents. Brain Res. *157*, 277–293.

Miao, C., Cao, Q., Ito, H.T., Yamahachi, H., Witter, M.P., Moser, M.-B., and Moser, E.I. (2015). Hippocampal remapping after partial inactivation of the medial entorhinal cortex. Neuron *88*, 590–603.

Miller, K.D. (1996). Synaptic economics: competition and cooperation in synaptic plasticity. Neuron *17*, 371–374.

Muller, R.U., and Kubie, J.L. (1987). The effects of changes in the environment on the spatial firing of hippocampal complex-spike cells. J. Neurosci. *7*, 1951–1968.

Muller, R.U., Kubie, J.L., Bostock, E., Taube, J., and Quirk, G. (1991). Spatial firing correlates of neurons in the hippocampal formation of freely moving rats. In Brain and Space, J. Paillard, ed. (Oxford University Press), pp. 296–333.

O'Keefe, J., and Dostrovsky, J. (1971). The hippocampus as a spatial map. Preliminary evidence from unit activity in the freely-moving rat. Brain Res. *34*, 171–175.

Pinault, D. (1996). A novel single-cell staining procedure performed in vivo under electrophysiological control: morpho-functional features of juxtacellularly labeled thalamic cells and other central neurons with biocytin or Neurobiotin. J. Neurosci. Methods *65*, 113–136.

Preston-Ferrer, P., and Burgalossi, A. (2017). Linking neuronal structure to function in rodent hippocampus: a methodological prospective. Cell Tissue Res. https://doi.org/10.1007/s00441-017-2732-7

Preston-Ferrer, P., Coletta, S., Frey, M., and Burgalossi, A. (2016). Anatomical organization of presubicular head-direction circuits. eLife *5*.

Ranck, J.B., Jr. (1973). Studies on single neurons in dorsal hippocampal formation and septum in unrestrained rats. I. Behavioral correlates and firing repertoires. Exp. Neurol. *41*, 461–531.

Rich, P.D., Liaw, H.-P., and Lee, A.K. (2014). Place cells. Large environments reveal the statistical structure governing hippocampal representations. Science *345*, 814–817.

Rueckemann, J.W., DiMauro, A.J., Rangel, L.M., Han, X., Boyden, E.S., and Eichenbaum, H. (2016). Transient optogenetic inactivation of the medial entorhinal cortex biases the active population of hippocampal neurons. Hippocampus *26*, 246–260.

Schoenenberger, P., O'Neill, J., and Csicsvari, J. (2016). Activity-dependent plasticity of hippocampal place maps. Nat. Commun. *7*, 11824.

Spiers, H.J., Hayman, R.M., Jovalekic, A., Marozzi, E., and Jeffery, K.J. (2015). Place field repetition and purely local remapping in a multicompartment environment. Cereb. Cortex *25*, 10–25.

Stüttgen, M.C., Nonkes, L.J.P., Geis, H.R.A.P., Tiesinga, P.H., and Houweling, A.R. (2017). Temporally precise control of single-neuron spiking by juxtacellular nanostimulation. J. Neurophysiol. *117*, 1363–1378.

Tang, Q., Brecht, M., and Burgalossi, A. (2014). Juxtacellular recording and morphological identification of single neurons in freely moving rats. Nat. Protoc. *9*, 2369–2381.

Trouche, S., Perestenko, P.V., van de Ven, G.M., Bratley, C.T., McNamara, C.G., Campo-Urriza, N., Black, S.L., Reijmers, L.G., and Dupret, D. (2016). Recoding a cocaine-place memory engram to a neutral engram in the hippocampus. Nat. Neurosci. *19*, 564–567.

Volgushev, M., Voronin, L.L., Chistiakova, M., and Singer, W. (1997). Relations between long-term synaptic modifications and paired-pulse interactions in the rat neocortex. Eur. J. Neurosci. *9*, 1656–1665.

Wilson, M.A., and McNaughton, B.L. (1993). Dynamics of the hippocampal ensemble code for space. Science *261*, 1055–1058.

Wu, Z., and Yamaguchi, Y. (2006). Conserving total synaptic weight ensures one-trial sequence learning of place fields in the hippocampus. Neural Netw. *19*, 547–563.

Cell Reports, Volume *23*

Supplemental Information

Manipulating Hippocampal Place Cell Activity by Single-Cell Stimulation in Freely Moving Mice

Maria Diamantaki, Stefano Coletta, Khaled Nasr, Roxana Zeraati, Sophie Laturnus, Philipp Berens, Patricia Preston-Ferrer, and Andrea Burgalossi

SUPPLEMENTAL FIGURES

FIGURE S1

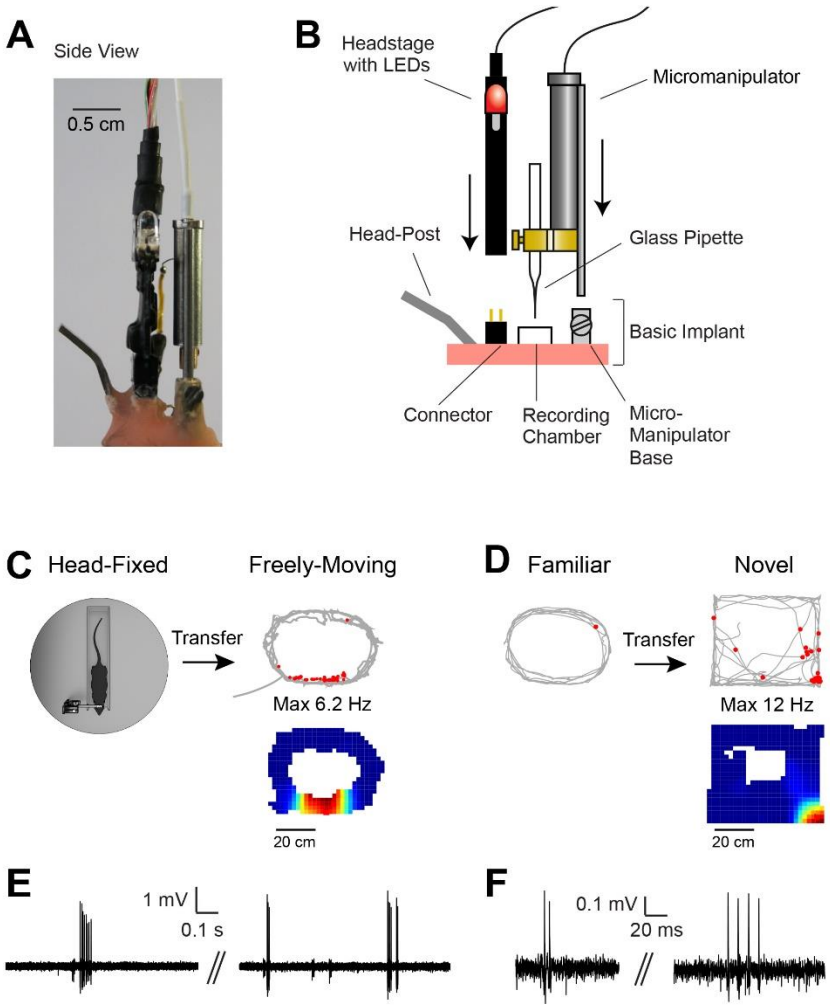

Figure S1. Mechanical stability of juxtacellular recordings in freely-moving mice (Related to Figure 1)

A. Side view of the fully-assembled recording implant.

B. Schematic drawing showing the components of the 'basic implant'(cemented on the mouse head) and the positioning of the micromanipulator and headstage (arrows) for performing juxtacellular recordings.

C. Left, schematic representation of a head-fixed mouse, which was released from head fixation and transferred to the behavioral arena (right) while maintaining the juxtacellular recording. Right, spike-trajectory plot (top) and rate map (bottom) for a representative neuron, showing place cell activity in the circular arena. Spontaneous spikes (red dots) and maximal firing rate are indicated.

D. Spike-trajectory plots (top) and rate map (bottom) showing the activity of a neuron, sequentially recorded across two different environments (familiar circular and novel square arenas). Spontaneous spikes (red dots) and maximal firing rate are indicated. The neuron was largely silent in the circular maze, while it displayed spatially-localized activity in the square arena. Note that, possibly due to the novelty of the environment, the animal's behavior was largely confined near the walls of the arena.

E-F. Representative high-pass filtered spike traces for the recordings shown in C and D, respectively.

FIGURE S2

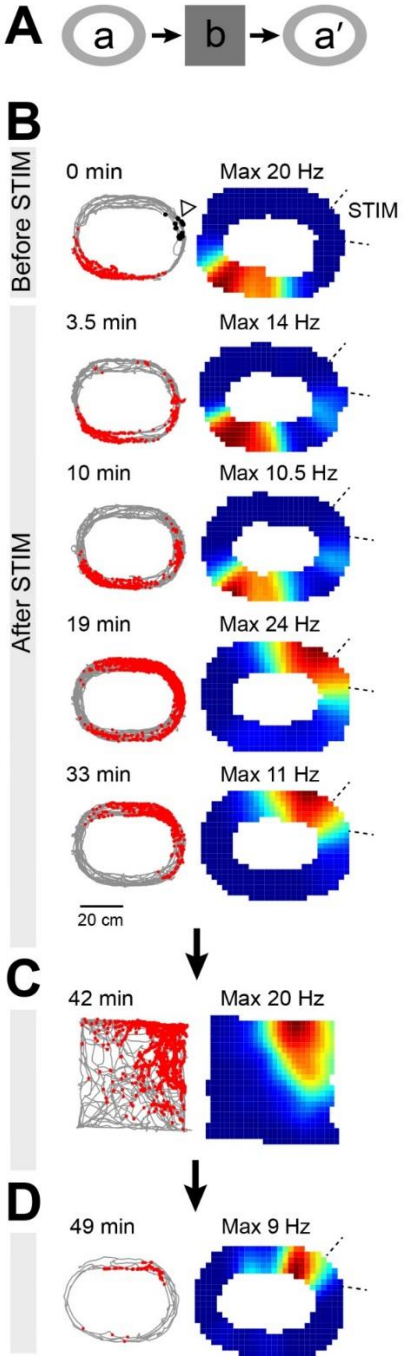
A
a
b
a′
B
Before STIM
0 min
Max 20 Hz
STIM
After STIM
3.5 min
Max 14 Hz
10 min
Max 10.5 Hz
19 min
Max 24 Hz
33 min
Max 11 Hz
20 cm
C
42 min
Max 20 Hz
D
49 min
Max 9 Hz

Figure S2. Monitoring of stimulation effects on place-cell activity after exposure to a different environment (Related to Figure 4)

A. Schematic representation of the experimental protocol, i.e. sequential recording of the same neuron in a circular (a), a square (b), and then back to the circular arena (a').

B. Spike-trajectory plots (left) and rate maps (right) during exploration of the circular arena (a). Top, spike-trajectory plot and rate map computed before the stimulation (before STIM). Stimulus spikes are indicated as black dots (arrowhead). Bottom, sequential recording of the same neuron in the circular arena at different time intervals following juxtacellular stimulation (after STIM). Stimulus spikes (black dots), spontaneous spikes (red dots), maximal firing rates and beginning of the recording times are indicated. The area containing the stimulus spikes is marked by dotted lines on the rate map. Note that as a place field gradually emerged at the stimulus location, the original place field became progressively weaker.

C. Spike-trajectory plot (left) and rate map (right) for the same neuron as in B, after the animal was transferred to a square arena (b). Maximal firing rate and beginning of recording time are indicated.

D. Same as in B, but after the mouse was placed back in the original circular arena (a'). Note the presence of the stimulation-induced place field.

FIGURE S3

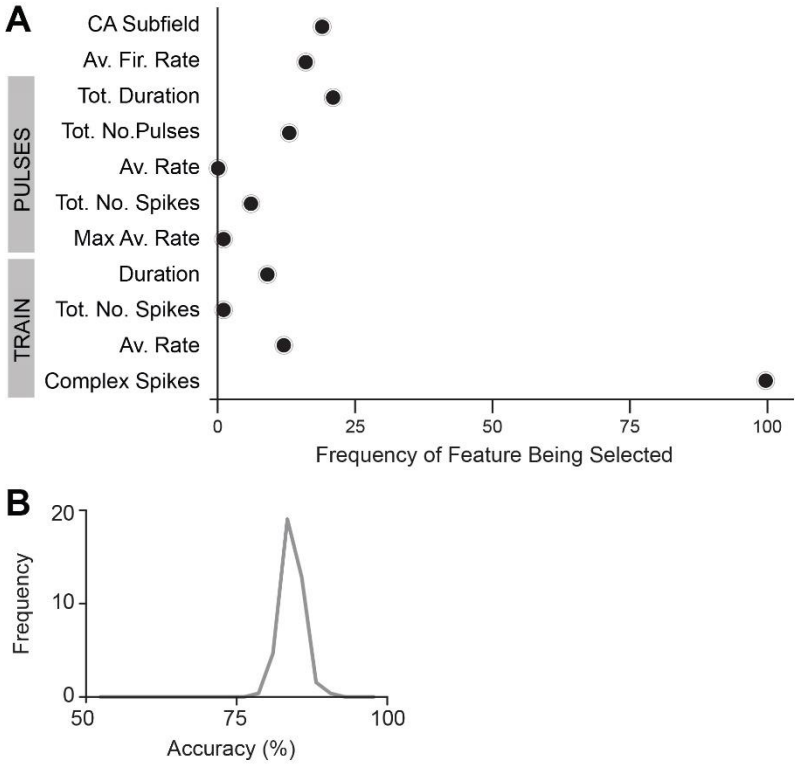

Figure S3. Effect prediction based on cellular/spike train features (Related to Figures 3 and 4)
A. A feature selection procedure on 100 synthetically balanced datasets indicates that among all tested features, the presence of complex spikes within evoked spike trains was most informative about the presence of the effect (i.e. the induction of spatial activity at the stimulus location). This feature was selected in all datasets, while all other features were selected in <25% of the datasets (see details in Supplemental Experimental Procedures).
B. Histogram over cross-validated average performance across 100 synthetically balanced datasets shows overall high predictive performance of cellular/spike train features for the occurrence of the effect (average 84.5 ± 10.9%, mean+-SD) (see details in Supplemental Experimental Procedures).

SUPPLEMENTAL EXPERIMENTAL PROCEDURES

All experimental procedures were performed according to the German guidelines on animal welfare under the supervision of local ethics committees.

Juxtacellular Recordings

Experimental procedures for obtaining juxtacellular recordings, signal acquisition and processing, and animal tracking were performed essentially as recently described (Tang et al., 2014; Diamantaki et al., 2016a). Briefly, glass pipette with resistance 4-6 MΩ were filled either with intracellular solution containing in mM: 135 K-gluconate, 10 HEPES, 10 Na_2-phosphocreatine, 4 KCl, 4 MgATP, and 0.3 Na_3GTP (pH was adjusted to 7.2) or standard Ringer solution containing in mM: 135 NaCl, 5.4 KCl, 5 HEPES, 1.8 $CaCl_2$ and 1 $MgCl_2$ (pH was adjusted to 7.2). In a subset of recordings, Neurobiotin (1.5-3%; Vector Laboratories, Cat.No. SP-1150) or Biocytin (1.5-3%; Sigma-Aldrich, Cat.No. Number 576-19-2) was added to the electrode solution. Osmolarity was adjusted to 290-320mOsm.

For juxtacellular recordings, C57BL/6J mice (RRID:IMSR_JAX:000664) were anesthetized with ketamine/xylazine, and surgery procedures were performed as previously described (Tang et al., 2014). Briefly, a custom-made recording chamber (diameter: 7.0mm, height: 2.5mm) was placed at the coordinates for targeting the dorsal hippocampus (see below) and filled with silicone sealant (Kwik-Cast, World Precision Instruments). In addition, a custom-made S-shaped metal head-post (length: 22mm, width: 3mm; 1 mm thick; **Figure 1A,B** and **Figure S1A,B**), and a 10-pins double-row connector (Buerklin, Cat.No. 58 F 542; length: 8mm, width: 3.2mm, height: 6.4mm) were implanted on the head of the mouse (see **Figure S1B**; 'basic implant') via a thin layer of UV-curable adhesive (Optibond All-In-One, Kerr; Cat.No. 34449E) and dental acrylic (Paladur – Kulzer). Animals were then slowly habituated to the head-fixation and to collect food pellets in a circular arena (outer dimensions 70x50cm and 9cm wide path) with 16cm high walls. A few recordings (**Figure S1** and **Figure S2**) were performed in a novel square arena (70x70cm, 22cm high walls). Prior to the recordings, a craniotomy was performed at the coordinates for targeting the dorsal hippocampus (1.5-2 mm posterior and 2-2.5 mm lateral from bregma), and a custom-made micromanipulator base (length: 3.9 mm; width: 2.7 mm, height: 8mm; **Figure 1A**) was cemented near the craniotomy for holding the micromanipulator. For performing juxtacellular recordings, the full recording implant was assembled, by securing the micromanipulator (Nanomotor, RRID:SCR_016100; diameter: 4mm, height: 16mm, travel distance: 9 mm; Kleindiek Nanotechnik) onto the head-mounted base (by means of a screw), and connecting the miniaturized head-stage (Miniature Headstage, RRID:SCR_016102; length: 6mm, width: 2.4mm, height: 20mm; NPI Electronic) to the pin connector (**Figure S1B**). By operating the micromanipulator, the glass electrode was slowly advanced under high-magnification stereomicroscopic guidance until it touched the surface of the brain (the dura was left intact). Then, the craniotomy was filled with a 2-3% solution (w/vol) of agarose solution (Roth, Cat.No. 9012-36-6; see Tang et al., 2014), the animal released from head-fixation and placed in the behavioral arena. Juxtacellular recordings in the dorsal hippocampus were established while animals explored the arena (for targeting procedures, see details in the paragraph below; see also Tang et al., 2014). Recordings were performed for up to 3 days following opening of the craniotomy (average, 1.5 ± 0.6 days). Overall recording efficiency – e.g. the average number of recordings (6.4 ± 6.0) and electrode penetrations per mouse (3.9 ± 2.7) – were similar to that reported for rats (Tang et al., 2014).

During both training and recordings, food pellets were thrown in the arena either manually by the experimenter or distributed automatically by a pellet dispenser (CT-ENV-203-5; Med Associates). In order to allow the animal to move freely in space during both training and recording sessions, the weight of the implant on the mouse's head was balanced by a counterweight system. All animals underwent the same training prior to the experiments (>5 days of habituation to the circular arena). To maximize spatial sampling within the limited juxtacellular recording durations, periods of rest/grooming between exploratory bouts were often minimized by encouraging mice to explore the arena (see Lee et al., 2012). Juxtacellular labeling was performed as previously described (Pinault, 1996; Diamantaki et al., 2016a;

Preston-Ferrer et al., 2016). The juxtacellular voltage signal was acquired via an ELC miniature headstage (NPI Electronic Miniature Headstage, RRID:SCR_016102), and an ELC-03XS amplifier (NPI Electronic, RRID:SCR_016038), sampled at 20–50kHz by a POWER1401-3 data-acquisition interface (CED, RRID:SCR_016040 CED) under the control of Spike2 v8.02 software. The location of the animal was tracked using two LEDs on the animal's head (red and blue with in-between distance of 2 cm). Animal tracking was performed by acquiring a video (25Hz frame rate) with the IC Capture Software (The Imaging Source).

Targeting of the hippocampus and cell identification

Before juxtacellular recordings, mapping experiments with low-resistance electrodes (0.5–1MΩ) were performed to precisely estimate the location of the dorsal CA1 and CA3 regions. Specifically, the occurrence of sharp-wave ripples complexes, their polarity reversal and the increased juxtacellular hit-rates served as reliable electrophysiological signatures for precisely localizing the CA1 pyramidal layer. Entry into the strata radiatum and lacunosum moleculare was usually associated with a drop in the electrode resistance and a progressive increase in the amplitude of LFP theta waves (Buzsáki, 2002). The beginning of the CA3 pyramidal layer could be mapped similar to the CA1 pyramidal layer, based on the increase in the electrode resistance (i.e. indicative of cell-contact) and increase in extracellular multi-unit activity. Thus electrode resistance, extracellular multi-unit activity, LFP theta, sharp-wave/ripple activity and juxtacellular hit-rates served as reliable correlates of the electrode location within the CA1/CA3 pyramidal layers. Indeed, cell identification was in large agreement with the expected electrode location. In all but one case (22 out of 23, see below) where the electrode was expected to be in the CA1 and CA3 pyramidal layers and juxtacellular labeling was performed, neurons within the CA1 or CA3 pyramidal layer were recovered. Only in one case a CA2 neuron was recovered (not included in further analysis). Based on this recovery rate, we cannot exclude that a subset of the stimulated neurons (~4%; estimated from our identified cell dataset) could potentially stem from the CA2 region. Recordings were classified as 'identified' if at least a soma and/or portions of the dendritic tree were recovered (see Burgalossi et al., 2011). Cell labelling was typically performed on the last electrode penetration, for obtaining additional confirmation of our targeting procedures; hence, a relationship between cell morphology and place field plasticity cannot be established from the present data.

Juxtacellular stimulation procedures

Juxtacellular stimulation of single neurons was performed according to previously established procedures, referred to as 'nanostimulation' (Houweling and Brecht, 2008; Houweling et al., 2010; Doron et al., 2014; Stüttgen et al., 2017). Briefly, single-cell stimulation was performed by applying positive square current pulses of 200ms duration and increasing amplitude (typically between 5 – 20nA) to elicit spikes during the ON phase of the pulses (**Figure 2A**). In some cases (23 out of 62 stimulations), in addition to evoking spikes during the ON phases, the pulse entrainment evoked a spike train, which exceeded the duration of the stimulation pulse (**Figure 2B**). Once evoked, spike trains lasted on average 7.0 ± 6.1s. These spike trains were possibly caused by strong depolarizations and/or transient access to the cell membrane potential (Diamantaki et al., 2016a). In a subset of the evoked spike trains (15 out of 23) we observed the presence of ramp-like depolarizations surmounted by short bursts of action potentials (**Figure 2B**); based on their characteristic attenuation of spike amplitudes, these events were classified as complex spikes. We note that strong somatic depolarizations are also used to experimentally evoke complex spikes in-vitro (Magee and Johnston, 1997) and in-vivo (Bittner et al., 2015) and during natural behavior, complex spikes are also accompanied by strong somatic depolarization (Epsztein et al., 2011). During pulse-entrainment, clear complex spikes were not observed; however, due to capacitive distortions of voltage traces during juxtacellular current injections, the possibility that a minority of complex spikes went undetected cannot be excluded. In total, for the stimulation dataset, 42 recordings were established from putative CA1 (n=21) and CA3 (n=21) pyramidal neurons: 20 spatially-modulated and 22 silent cells. While the putative anatomical location of the neurons (CA1 versus CA3) did not have a significant effect on classification accuracy (see **Figure S3**), the limited number of observations prevents to formally rule out possible

structure-function relationships. Some neurons were stimulated multiple times at the same location (9 neurons stimulated 2 times, 1 stimulated 3 times, 3 stimulated 4 times), but no obvious correlation was found between the number of stimulations and the probability of inducing a place field (not shown).

Histochemistry and cell reconstruction

At the end of each recording, the animal was euthanized with an overdose of pentobarbital and perfused transcardially with 0.1M phosphate-buffered saline followed by a 4% paraformaldehyde solution. Brains were cut on vibratome to obtain 70μm thick coronal sections. To reveal the morphology of juxtacellularly labeled cells, brain slices were processed with streptavidin-546 (Thermo Fisher Scientific, Cat.No. S11225) as previously described (Tang et al., 2014). Immunohistochemical stainings for Purkinje cell protein 4 (PCP4, Sigma-Aldrich, Cat.No. HPA005792) were performed on free-floating sections as previously described (Ray et al., 2014) for identifying the anatomical boundaries of the CA2 region (Kohara et al., 2014; San Antonio et al., 2014). After fluorescence images were acquired, the neurobiotin/biocytin staining was converted into a dark DAB reaction product. Neuronal reconstructions were performed manually on DAB-converted specimens with the Neurolucida software (MBF Bioscience) and displayed as 2-dimensional projections.

Analysis of Electrophysiology Data

A three-dimensional analysis using time and the first two principal components of the waveform was performed to visualize and assess the stability of spikes amplitude over time, and to isolate spikes from recording artifacts (as in Burgalossi et al., 2011). On average, our peak-to-peak spike amplitudes were 2.4 ± 1.1 mV, which corresponded to 45 ± 23 times above the root mean square amplitude of the noise (n=87). The beginning and end of the stimulation interval were defined as the time between the first and the last evoked spikes. For pulse-entrainment, the following features were quantified: total duration (defined as the sum of the ON times where evoked spikes were observed), total number of stimulation pulses, average firing rate of the evoked spikes, total number of spikes and maximal firing rate (defined as the highest firing rate among all ON pulses that evoked spikes). For the evoked spike trains, the following features were quantified: total duration, average firing rate, total number of spikes and presence of complex spikes. These stimulus features were used for logistic regression analysis (see 'Logistic Regression Classification' paragraph below). The 'stimulated area', marked by dotted lines in **Figure 4A,C** and **Figure S2** was defined as the region of the circular arena containing all stimulus spikes. Stimulation effects were quantified based on the pixel by pixel firing rate correlations of the rate maps before and after the stimulations (**Figure 4D**). Effect latencies were defined as the time between the first stimulus spike and the first spontaneous spike at the stimulus location following stimulation. Recordings (or portions of recordings) in which cellular damage was observed (e.g. spike-shape broadening, increase in firing rate accompanied by negative DC-shifts of the juxtacellular voltage signal, as described in (Pinault, 1996; Herfst et al., 2012) were excluded from the analysis.

Statistical significance was assessed by Wilcoxon signed-rank test with 95% confidence intervals. All data are presented as mean ± st.dev. unless indicated otherwise.

Analysis of Spatial Modulation

Animal positional coordinates were extracted from the video (Format: AVI, Frame rate: 25Hz) by a custom-made software written in MATLAB, as previously described (Diamantaki et al., 2016a; Diamantaki et al., 2016b). Briefly, after calculating the LED positions frame by frame, the position of the mouse was defined as the midpoint between two head-mounted LEDs. For calculating rate maps, space was discretized into pixels of 2.5cm x 2.5cm, for which the occupancy *z* of a given pixel *x* was calculated as

$$z(x) = \sum_{t} w(|x - x_t|)\Delta t$$

where x_t is the position of the rat at time t, Δt the inter-frame interval, and w a Gaussian smoothing kernel with σ = 2.5cm.
Then, the firing rate r was calculated as

$$r(x) = \frac{\sum_i w(|x - x_i|)}{z}$$

where x_i is the position of the mouse where spike i was fired. The firing rate of pixels, whose occupancy z was less than 20ms, was considered unreliable and not shown. Spike fired at speed < 1 cm/s were not included in the spatial analysis.
Recordings were considered 'active' if their average firing rate was > 0.1 Hz, and were included in the spatial analysis on the basis of spatial coverage criteria (≥3 laps). Neurons were classified as place cells if the place-field peak firing rate was > 1 Hz and the place field size accounted for >10% and <40% of the total visited pixels. Place field side was defined as all contiguous pixels with average firing rate exceeding 20% of the peak firing rate (Ranck, 1973; Muller et al., 1987). The 'in-field firing rate' (**Figure 4E**) was calculated as the average firing rate over all place field pixels. For the linearized rate maps and trajectories, the X-Y coordinates were first converted into a 1-dimensional representation. This was done by first projecting the X-Y coordinates onto the ellipse that best-approximated the trajectory, and then converting the projected coordinates into a 1-dimensional representation by finding their associated positions along the linearized ellipse.

Logistic Regression Classification
To test whether the stimulation effect (i.e. the induction of spatial activity at the stimulus location) was related to cellular and evoked activity parameters (see **Figure S3A**), we used a logistic regression classifier with L2-regularization using the *glmnet* toolbox for Python (α = 0). The following features were used: total duration, total number of stimulation pulses, average firing rate, total number of spikes and maximal firing rate (for pulse-entrainment); total duration, average firing rate, total number of spikes and presence of complex spikes (for the evoked spike trains); anatomical location (CA1 versus CA3) and neuronal average firing rate (see **Figure S3**). Stimulations (n=62) were defined as 'effect' if they evoked spontaneous activity within the stimulus location (16 out of 62 stimulations). 60 stimulations evoked spikes on the ON-phase of the current pulses ('pulse entrainment'), 21 of which also evoked action potential trains ('evoked AP train'), and 2 stimulations only evoked a spike train (see **Figure 2**). The optimal classifier is found by minimizing:

$$\min_{\beta \in R^{p+1}} - \left[\frac{1}{N}\sum_{i=1}^{N} y_i \cdot \left(x_i^T \beta\right) - \log\left(1 + e^{-x_i^T \beta}\right)\right] + \lambda \|\beta\|_2^2$$

Straightforward application of this classification setup was complicated by two issues: (i) The severe class imbalance (only 16 'effect' stimulations out of 62) complicates the interpretation of the classification result, as already smart guessing can achieve an accuracy of 75% by solely assigning each data point to the 'no effect' class. To overcome this problem, we employed synthetic minority over-sampling (SMOTE; Lemaitre et al., 2017). SMOTE synthesizes new samples by interpolating between one sample x_i of the minority class and a randomly picked sample $x_{z(i)}$ in x_i`s k nearest-neighbor neighborhood (here k=5).

$$x_{new} = x_i + \gamma(x_{z(i)} - x_i)$$

The mixing coefficient γ is drawn from a uniform distribution between 0 and 1. This makes classification boundaries smoother than with random oversampling with replacement. Using SMOTE, we generated 100 balanced data sets. (ii) Correlations between features can impair the interpretability of the coefficient

vector. To study which features are predictive of the effect, we used cross-validated recursive feature elimination (RFECV) introduced by (Guyon et al., 2002) and implemented in the respective function in *sklearn*. This method trains a classifier first on the full set of features and then recursively prunes away features with low coefficients. The subset of features that gives the least averaged error across all training folds is returned as final set.

The complete procedure, thus, works as follows: we generated 100 balanced data sets using SMOTE and evaluated their average cross-validated classification accuracy using 10-fold cross-validation (see **Figure S3B**). Afterwards, we performed 10-fold RFECV on 100 newly generated data sets to obtain pruned feature vectors for each. Each feature's selection frequency can be seen in **Figure S3A**.

SUPPLEMENTAL REFERENCES

Bittner KC, Grienberger C, Vaidya SP, Milstein AD, Macklin JJ, Suh J, Tonegawa S, Magee JC (2015) Conjunctive input processing drives feature selectivity in hippocampal CA1 neurons. Nature neuroscience 18:1133-1142.

Burgalossi A, Herfst L, von Heimendahl M, Förste H, Haskic K, Schmidt M, Brecht M (2011) Microcircuits of Functionally Identified Neurons in the Rat Medial Entorhinal Cortex. Neuron 70:773-786.

Buzsáki G (2002) Theta oscillations in the hippocampus. Neuron 33:325-340.

Diamantaki M, Frey M, Preston-Ferrer P, Burgalossi A (2016a) Priming spatial activity by single-cell stimulation in the dentate gyrus of freely moving rats. Current Biology 26:536-541.

Diamantaki M, Frey M, Berens P, Preston-Ferrer P, Burgalossi A (2016b) Sparse activity of identified dentate granule cells during spatial exploration. eLife 5:e20252.

Doron G, von Heimendahl M, Schlattmann P, Houweling AR, Brecht M (2014) Spiking irregularity and frequency modulate the behavioral report of single-neuron stimulation. Neuron 81:653-663.

Epsztein J, Brecht M, Lee AK (2011) Intracellular determinants of hippocampal CA1 place and silent cell activity in a novel environment. Neuron 70:109-120.

Guyon I, Weston J, Barnhill S, Vapnik V (2002) Gene selection for cancer classification using support vector machines. Machine learning 46:389-422.

Herfst L, Burgalossi A, Haskic K, Tukker JJ, Schmidt M, Brecht M (2012) Friction-based stabilization of juxtacellular recordings in freely moving rats. Journal of neurophysiology 108:697-707.

Houweling AR, Brecht M (2008) Behavioural report of single neuron stimulation in somatosensory cortex. Nature 450.

Houweling AR, Doron G, Voigt BC, Herfst LJ, Brecht M (2010) Nanostimulation: manipulation of single neuron activity by juxtacellular current injection. Journal of neurophysiology 103:1696-1704.

Kohara K, Pignatelli M, Rivest AJ, Jung H-Y, Kitamura T, Suh J, Frank D, Kajikawa K, Mise N, Obata Y (2014) Cell type-specific genetic and optogenetic tools reveal hippocampal CA2 circuits. Nature neuroscience 17:269-279.

Lee D, Lin B-J, Lee AK (2012) Hippocampal Place Fields Emerge upon Single-Cell Manipulation of Excitability During Behavior. Science 337:849-853.

Lemaitre G, Nogueira F, Aridas CK (2017) Imbalanced-learn: A python toolbox to tackle the curse of imbalanced datasets in machine learning. Journal of Machine Learning Research 18:1-5.

Magee JC, Johnston D (1997) A synaptically controlled, associative signal for Hebbian plasticity in hippocampal neurons. Science 275:209-213.

Muller R, Kubie J, Ranck J (1987) Spatial firing patterns of hippocampal complex-spike cells in a fixed environment. The Journal of Neuroscience 7:1935-1950.

Pinault D (1996) A novel single-cell staining procedure performed in vivo under electrophysiological control: morpho-functional features of juxtacellularly labeled thalamic cells and other central neurons with biocytin or Neurobiotin. Journal of neuroscience methods 65:113-136.

Preston-Ferrer P, Coletta S, Frey M, Burgalossi A (2016) Anatomical organization of presubicular head-direction circuits. eLife 5:e14592.

Ranck JB (1973) Studies on single neurons in dorsal hippocampal formation and septum in unrestrained rats: Part I. Behavioral correlates and firing repertoires. Experimental Neurology 41:462-531.

Ray S, Naumann R, Burgalossi A, Tang Q, Schmidt H, Brecht M (2014) Grid-layout and theta-modulation of layer 2 pyramidal neurons in medial entorhinal cortex. Science 343:891-896.

San Antonio A, Liban K, Ikrar T, Tsyganovskiy E, Xu X (2014) Distinct physiological and developmental properties of hippocampal CA2 subfield revealed by using anti-Purkinje cell protein 4 (PCP4) immunostaining. Journal of Comparative Neurology 522:1333-1354.

Stüttgen MC, Nonkes LJ, Geis HRA, Tiesinga PH, Houweling AR (2017) Temporally precise control of single-neuron spiking by juxtacellular nanostimulation. Journal of neurophysiology 117:1363-1378.

Tang Q, Brecht M, Burgalossi A (2014) Juxtacellular recording and morphological identification of single neurons in freely moving rats. Nat Protocols 9:2369-2381.